International Journal of Advances in Electrical Engineering

E-ISSN: 2708-4582
P-ISSN: 2708-4574
IJAEE 2025; 6(1): 45-54

www.electricaltechjournal.com
Received: 05-01-2025
Accepted: 09-02-2025

M Bhanu Prakash
Assistant Professor, Department of EEE, Usha Rama College of Engineering and Technology, Telaprolu, Andhra Pradesh, India

Mounisha Ammla
UG Scholar, Department of EEE, Usha Rama College of Engineering and Technology, Telaprolu, Andhra Pradesh, India

G Harsha Vardhan
UG Scholar, Department of EEE, Usha Rama College of Engineering and Technology, Telaprolu, Andhra Pradesh, India

V Pradeep
UG Scholar, Department of EEE, Usha Rama College of Engineering and Technology, Telaprolu, Andhra Pradesh, India

Correspondence
M Bhanu Prakash
Assistant Professor, Department of EEE, Usha Rama College of Engineering and Technology, Telaprolu, Andhra Pradesh, India

An accurate loss model of single-stage single phase isolated PFC converter for bidirectional plug-in EV charger

M Bhanu Prakash, Mounisha Ammla, G Harsha Vardhan and V Pradeep

DOI: https://www.doi.org/10.22271/27084574.2025.v6.i1a.85

Abstract
In recent years, the power handling capability of EV chargers has been growing to reduce the charging time. In order to enhance the design and efficiency of EV chargers, an in-depth investigation of the losses caused in plug-in EV chargers is needed. This article presents an accurate loss model of a novel single-stage single-phase isolated PFC converter for a bidirectional EV charging application. The EV charger includes a current-fed full bridge converter with bidirectional switches on the grid side with a swinging boost inductor that is affiliated with a full bridge converter at the DC-side coupled via a high-frequency transformer. The AC-side current can be controlled to obtain power factor correction with low current total harmonic distortion (THD). The AC-side switches are naturally commutated and attained zero current switching (ZCS) without any external passive components. Additionally, zero current turn- ON is accomplished for DC-side switches to realize a high-efficiency EV charger. This is achieved with a modified control strategy and novel modulation method are adopted for achieving soft switching operation and bidirectional power flow. To ensure that the proposed EV charger is feasible, experimental results with loss analysis of a 1.5 kVA unit are presented showing that the operation, analysis, and design are perfectly accorded.

Keywords: EV Charger, wide bandgap device-based EV charger, Single-Stage Bidirectional Charger, Power Factor Correction (PFC), Isolated AC/DC Converter

Introduction
The global automotive industry is witnessing a significant shift from internal combustion engine (ICE) vehicles to battery electric vehicles (BEVs), with the market share of ICE vehicles expected to decline substantially over the coming years [1]. This growing penetration of BEVs necessitates the rapid expansion and enhancement of EV charging infrastructure. Among the emerging technologies, bidirectional EV chargers have become increasingly important due to their potential to support the grid during peak demand periods. The integration of smart grid technologies and renewable energy sources has further amplified the relevance of bidirectional chargers compared to their unidirectional counterparts [2]. EV chargers are broadly classified into on-board and off-board types. On-board chargers are integrated into the vehicle and typically used for home or residential charging. Off-board chargers, on the other hand, are installed at public or workplace charging stations and are not embedded in the vehicle itself [3]. The conventional EV charger architecture typically follows a two-stage conversion topology, consisting of a front-end boost PFC (power factor correction) AC-DC stage followed by an isolated DC-DC conversion stage, as shown in Fig. 1(a). These designs require a large DC-link capacitor, usually electrolytic, between the two stages. While electrolytic capacitors provide necessary energy buffering, they are prone to a higher failure rate, thereby compromising system reliability and increasing both size and cost [4].

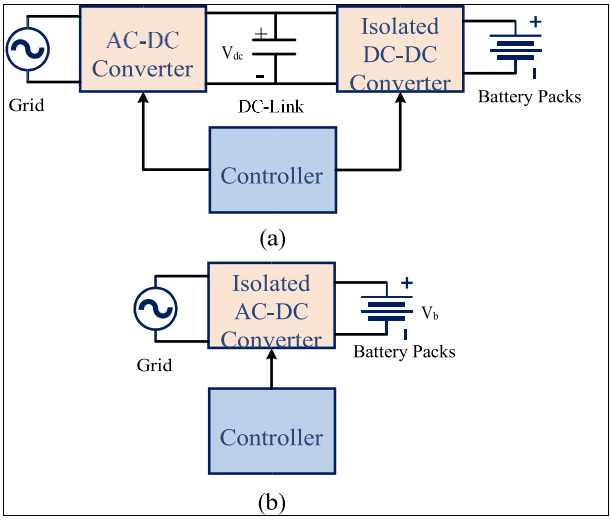

These converters offer higher power density and component reduction, making them suitable for compact and cost-effective EV charging applications [5].

Various bridgeless PFC topologies have been proposed to reduce conduction losses [6-8], but these often suffer from increased component count and electromagnetic interference (EMI). Recent advancements in wide bandgap (WBG) devices have led to the development of totem-pole PFC converters, which exhibit lower EMI, reduced conduction losses, and enhanced power density [9], [10]. A hybrid converter that combines a half-bridge and symmetric full-bridge topology was introduced in [11], which achieves improved efficiency due to reduced circulating current and a lower transformer turns ratio.

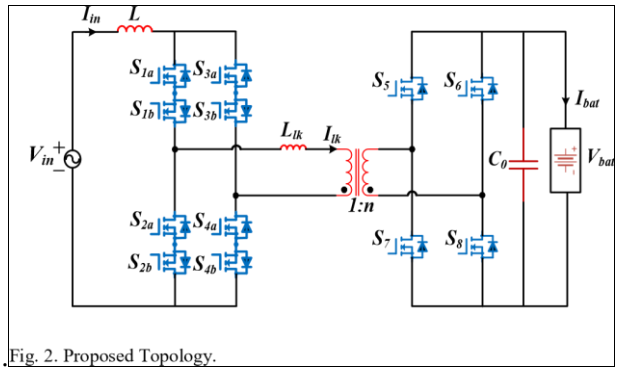

Fig. 2. Proposed Topology.

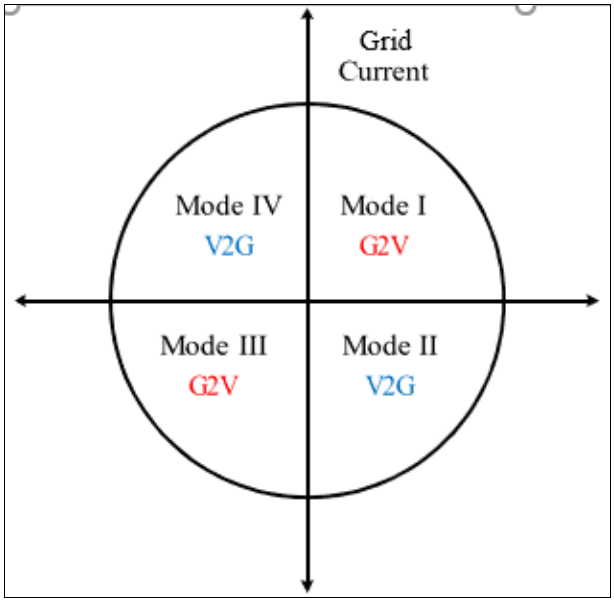

A current-fed bidirectional isolated single-stage PFC converter, as discussed in [12] and derived from concepts in [13], offers several advantages: galvanic isolation, improved current shaping at the AC grid interface, and reduced switching losses. These converters are particularly appealing due to their inherent short-circuit protection, low leakage inductance, reduced copper and duty-cycle losses, and lower peak and RMS currents through the switches [14].

Proposed Topology and Operating Principle

This paper proposes a novel secondary-modulation-based, naturally clamped, soft-switching, single-stage bidirectional isolated PFC converter for electric vehicle charging applications, as depicted in Fig. 2. The proposed system includes a current-fed full-bridge converter on the AC side with back-to-back bidirectional switches, and a full-bridge converter on the DC side connected to the EV battery. These two stages are coupled through a high-frequency transformer (HFT), providing galvanic isolation.

The AC-side switches achieve inherent zero-current switching (ZCS) without the need for external snubber circuits, while the DC-side switches operate under zero-current turn-on conditions, reducing switching losses and enhancing system efficiency. The converter achieves soft-switching across the entire operating range without requiring additional passive or active components.

Moreover, the design incorporates a boost inductor, whose magnetic characteristics—including core permeability and physical dimensions—are analyzed in detail. An accurate loss model is developed to evaluate the oscillatory behavior of the boost inductor current over the entire AC grid cycle. The performance of the converter is further evaluated based on efficiency metrics under various load conditions and total harmonic distortion (THD) of the input grid current.

varying thermal conditions ranging from 10°C to 80°C. Software tools, including MATLAB R2022a and Python 3.9, were utilized to implement, simulate, and validate the gamma adjustment algorithms. Thermal imaging was conducted using a FLIR T540 infrared thermal camera to visualize and record temperature gradients during prolonged operation. Data acquisition and control were managed using an Arduino Mega 2560 microcontroller.

Operation

The operation of the proposed single-stage bidirectional isolated converter depends on the polarity of the grid voltage and current. It is capable of seamless bidirectional power transfer between the grid and electric vehicle battery, supporting both active and reactive power flow. Based on the direction of power transfer and the instantaneous grid voltage polarity, the converter operates in four distinct modes. This section presents a detailed explanation of Mode I (G2V) and Mode II (V2G) operations.

Mode I (G2V Mode): Converters operate in mode I when the ac voltage is in the positive half cycle and energy is being transferred from the grid to the battery. On the ac side are driven by duty ratio modulation as shown in Fig. 4, whereas S_{1a}, S_{4a}, and S_{2a}, S_{3a} conduct at high frequency with d_1 modulation, and the gate pulses of the two phases are 180^{θ} out of phase, as shown in Fig. 4. To ensure that the conductance of S_{1a}, S_{4a}, and S_{2a}, S_{3a} overlaps, the duty cycle d_1 is maintained between 0.5 to 1. As long as the grid voltage is positive, the remaining ac-side switches S_{1b}, S_{2b}, S_{3b}, and S_{4b} will remain ON. The semiconductor switches on

the dc side have a constant duty cycle d_r, and the secondary side switches S_5, S_6, S_7, and S_8 that are switched off are connected to the grid side. By switching off S_{2a} and S_{3a}, the grid current is routed via S_{1a} and S_{4a}. HFT is used to swap the current flowing between the ac-side and dc-side. During turn ON of S_{2a} and S_{3a} causes a linear transfer of current from the HFT to the active device; the current then gradually declines via S_{1a} and S_{4a} to reach $I_{in}/2$. The body diodes of switches S_6 and S_7 on the DC-side can achieve zero current through them. In order to achieve ZCS, secondary-side semiconductor devices are used to reduce the current at grid-side semiconductor devices, which are naturally switched-OFF. With gained primary HFT voltage $-V_0/$ is accomplished by gating the switches S_6 and S_7 immediately before to turning ON the grid side switches. The current via grid-side devices will be at zero when the switches are turned off, and this may be guaranteed by monitoring the duty cycle d_r of the battery-side switches. Additionally, it reduces the peak current drawn by the opposite leg of grid side. The voltage waveforms on the main and secondary sides of an HFT are shown in Fig. 4, together with the waveforms of the ac-side and dc-side switches, respectively.
In [15], the detailed operation of Mode-I is explained for isolated bidirectional dc-dc converter of fuel-cell application. The output voltage is derived as;

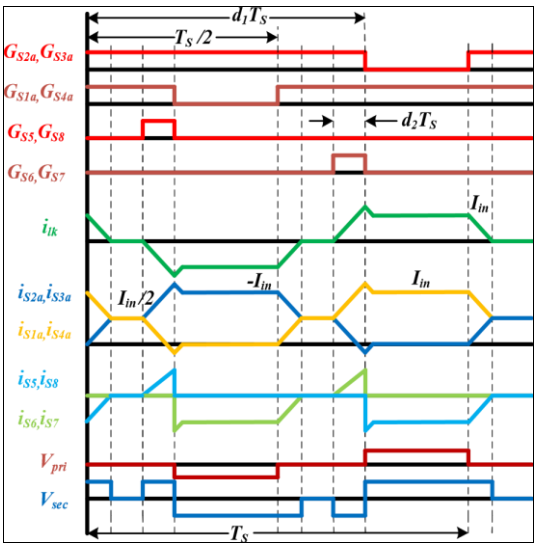

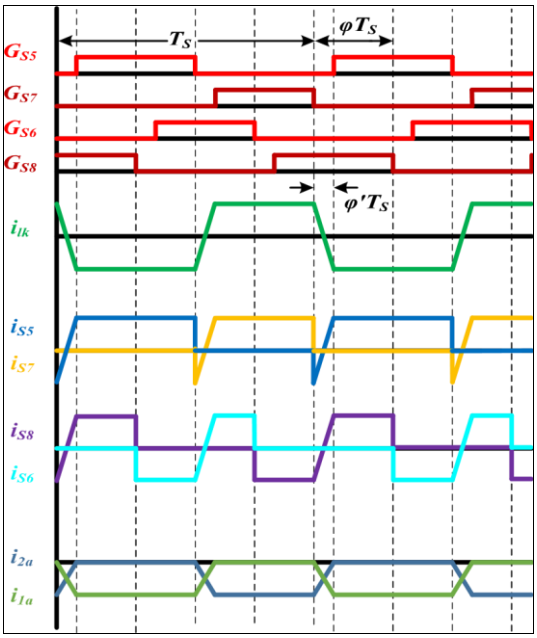

Mode II (V2G Mode): In mode-II, the power is transferred from the vehicle battery to the grid. Negative ac-grid current keeps semiconductor switches and on the AC, side continued ON, while the same current keeps switches, and are continued-OFF mode. This mode has the phase shift in the gate signal between the two legs, as converter functioning as a standard isolated voltage-fed full bridge converter with an inductive output filter. By inducing
shown in Fig. 5, the voltage across the transformer is adjusted. On the battery-side, the gate signals from the top and bottom devices complement one another. In this operation, output.

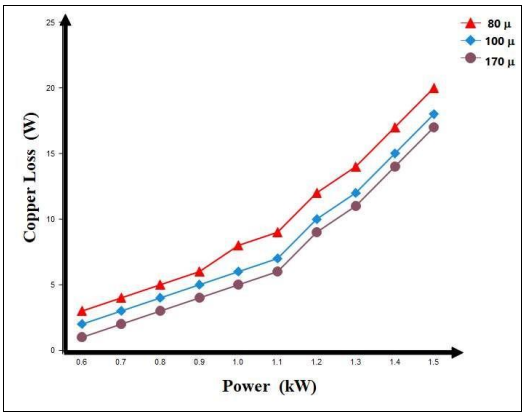

Where is the amount of time it takes for the value of to change from positive to negative and vice versa, as shown in Fig. 5? The battery-side dead time between top and bottom switches is precisely chosen to ensure zero voltage switching (ZVS). The ac-grid side switches, and diodes of the switches, and are conducted for flowing the current towards ac-side. ZCS is made plausibly steady and consistent which resulting into increasing the efficiency of the converter.

Mode III (G2V Mode): Power is sent from the grid to the battery storage of vehicle during this mode. The primary active switches on the ac-side S_{1b}, $S_{4b,}$ and S_{2b}, S_{3b}, are functioned at higher frequency with d_1 modulation, and the gate pulses of the two phases are 180° out of phase as a result of negative grid voltage and current. The duty cycle d_1 is preserved between 0.5 to 1 and the conductance of S_{1b}, $S_{4b,}$ and S_{2b}, S_{3b} overlaps.
Switches S_{1a}, S_{2a}, S_{3a}, and S_{4a} on the ac-side are continued ON. The secondary-side switches S_5, S_6, S_7, and S_8 are connected to ac-side semiconductor switches with the duty cycle d_r which is fixed for dc-side switches. To get the voltage at the ac-side HFT, the gate signals on the DC side are switched using swapped Mode-I. Switches S_5 and S_8 on the DC side are turned OFF at the same time as S_{1b} and S_{4b}. Switches S_{2b} and S_{3b} are turned-OFF at the same time as S_6 and S_7. When S_{1b}, S_{4b} and S_{2b}, S_{3b} are being switched-OFF, the current flowing through primary devices decreases to zero and, ZCS operation achieves.
When the current increases linearly from zero, the turn-on losses = − 2. (1 −.) (3)
are reduced. The output voltage is given as,

Mode IV (V2G Mode): During this mode, positive grid current and negative grid voltage transmit power from battery storage of vehicle to the grid. The current is flowing through the diodes of devices and switches. The phase shift modulation (PSM) method is also used to control and regulate switches on the DC-side.

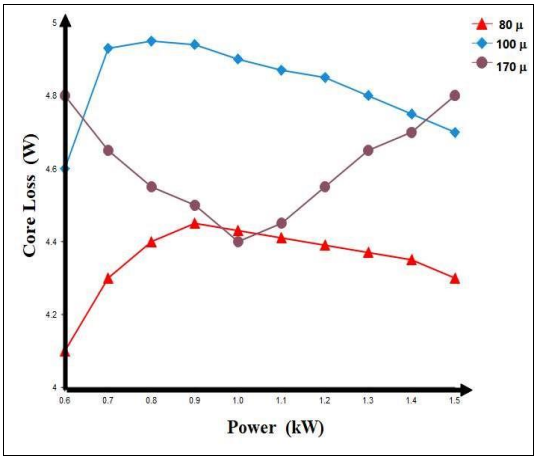

The proposed single-stage, bidirectional, isolated PFC converter demonstrates robust and flexible operation under all grid conditions through its four-mode control strategy.

Modes I and III facilitate grid-to-vehicle (G2V) charging during the positive and negative half-cycles of the grid voltage, respectively, while Modes II and IV support vehicle-to-grid (V2G) discharging for bidirectional power flow.

The current-fed full-bridge topology ensures natural zero-current switching (ZCS) on the AC side and zero-current turn-on on the DC side, thereby minimizing switching losses and improving system efficiency. Through appropriate modulation strategies—duty-ratio control in G2V modes and phase-shift control in V2G modes—the converter achieves soft-switching operation across the full operating range without requiring additional passive components.

This versatile operation, along with galvanic isolation via the high-frequency transformer and accurate power flow control, makes the proposed topology highly suitable for next-generation EV charging infrastructures, supporting both fast charging and grid-interactive functions.

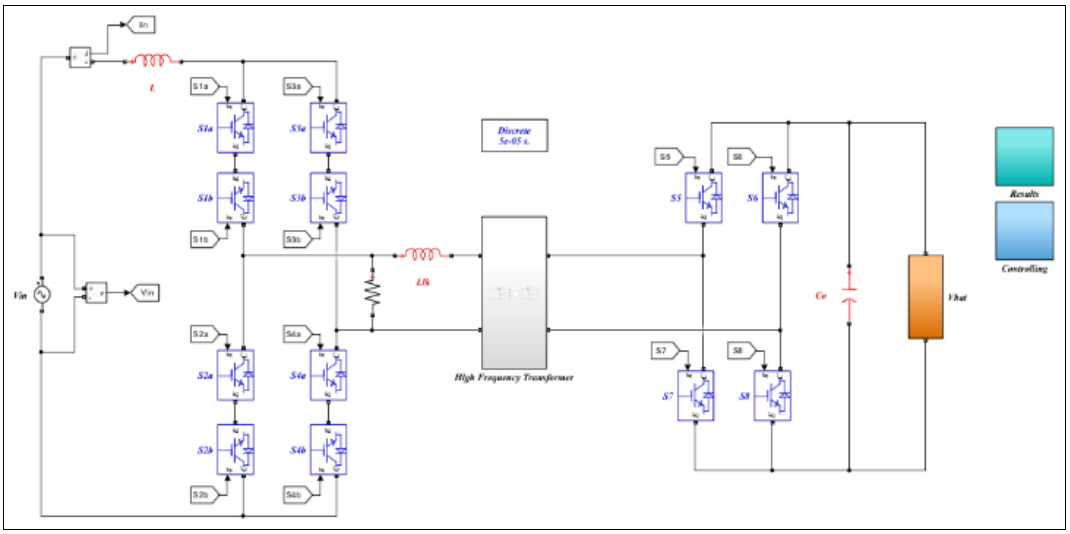

Fig 1: Simulation diagram

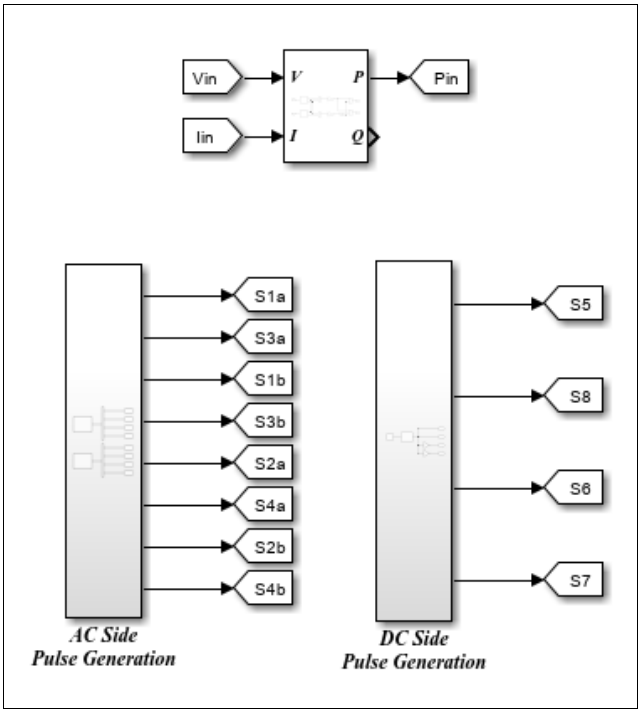

Fig 2: Open-Loop Controlling

Case 1: Grid-vehicle operation

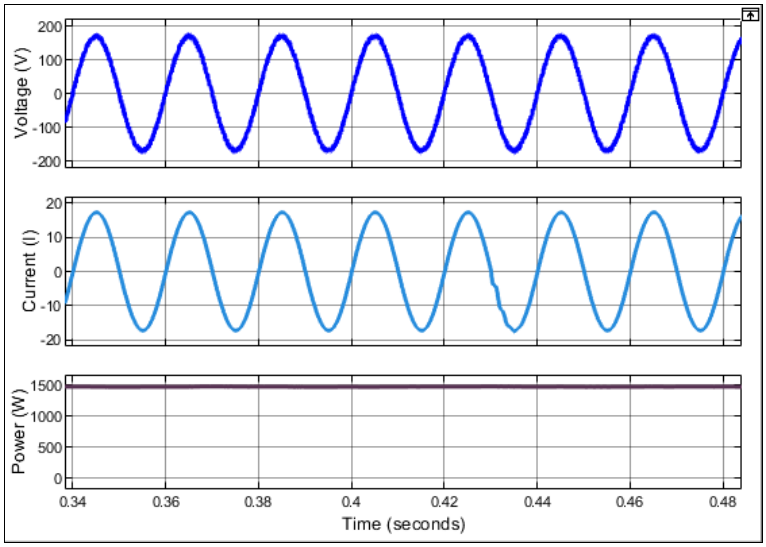

Fig 3: Grid Voltage, Current & Power

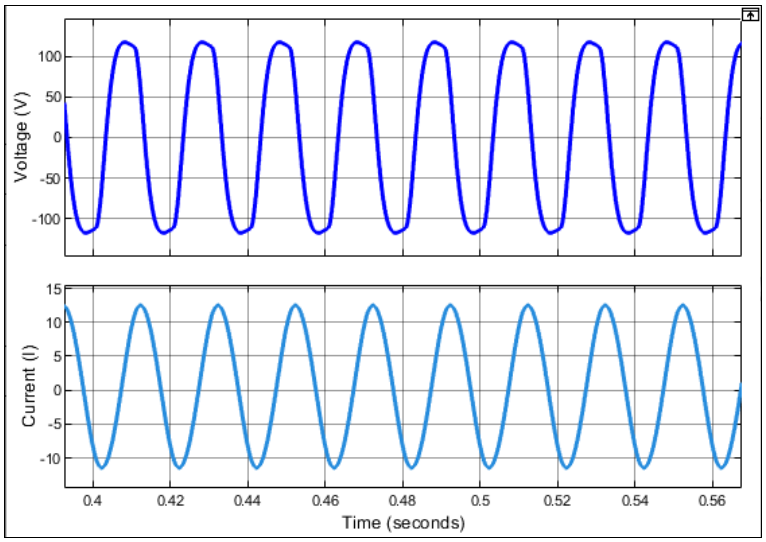

Fig 4: Primary Side Voltages & Currents

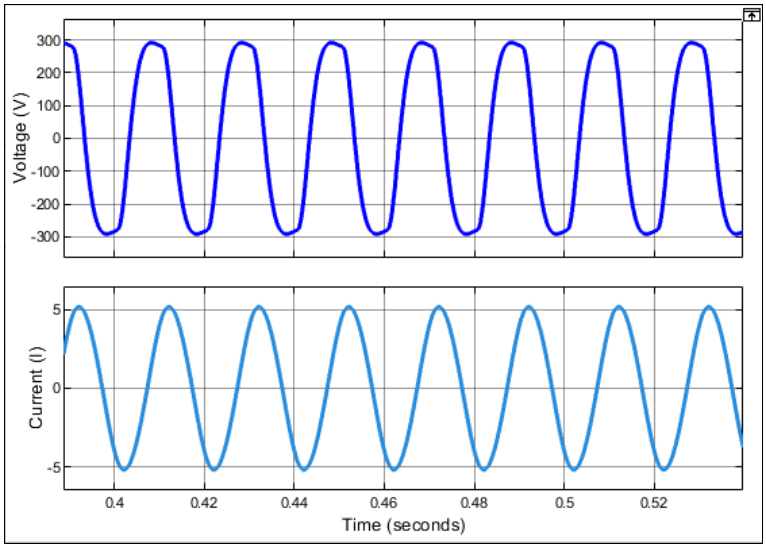

Fig 5: Secondary Side Voltages, Currents

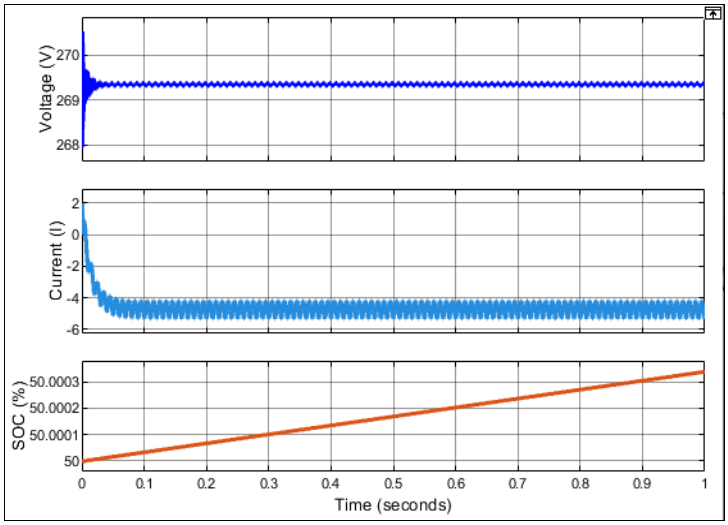

Fig 6: Battery Voltage, Current & SOC

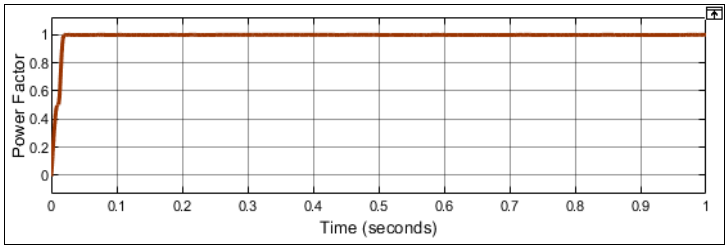

Fig 7: Power Factor

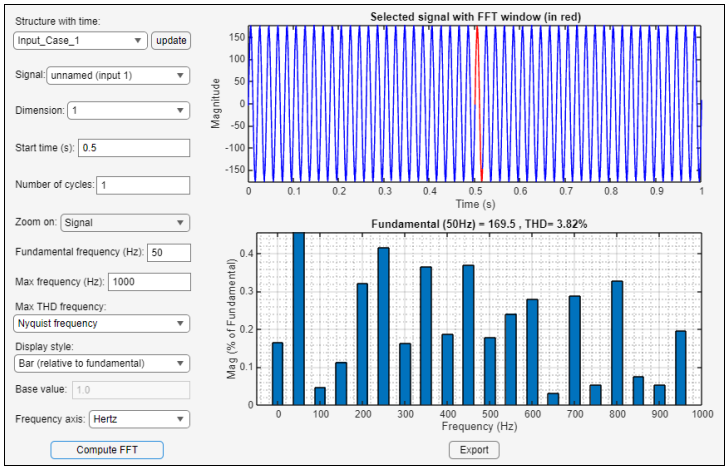

Fig 8: THD's in Grid Voltage

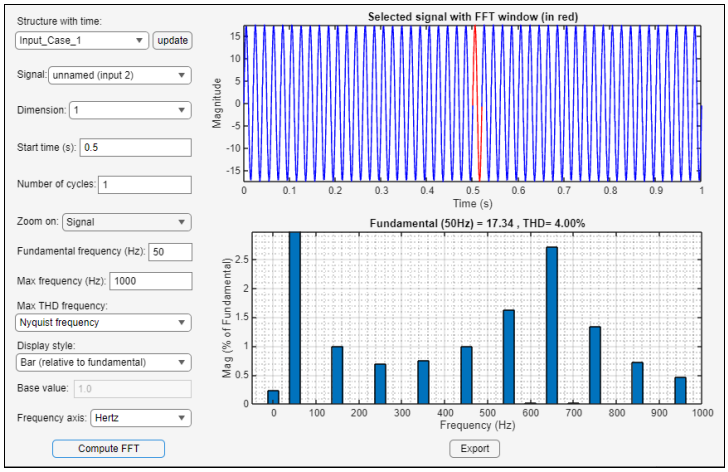

Fig 9: THD's in Grid Current

In the Grid-to-Vehicle (G2V) mode, power from the AC grid is converted into DC (direct current) through an AC-DC converter. This DC power is then used to charge the battery of the electric vehicle (EV). The process ensures that the vehicle's battery is replenished with energy when connected to the grid.

Case 2: Vehicle-grid operation

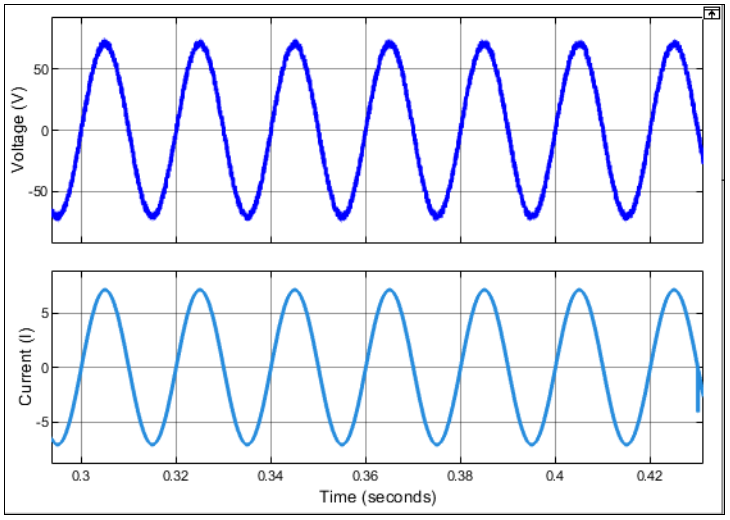

Fig 10: Grid Voltage, Current

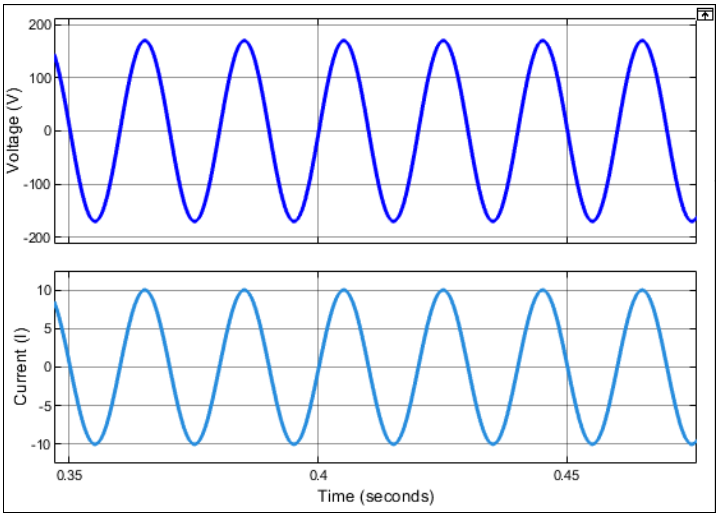

Fig 11: Primary Side Voltages & Currents

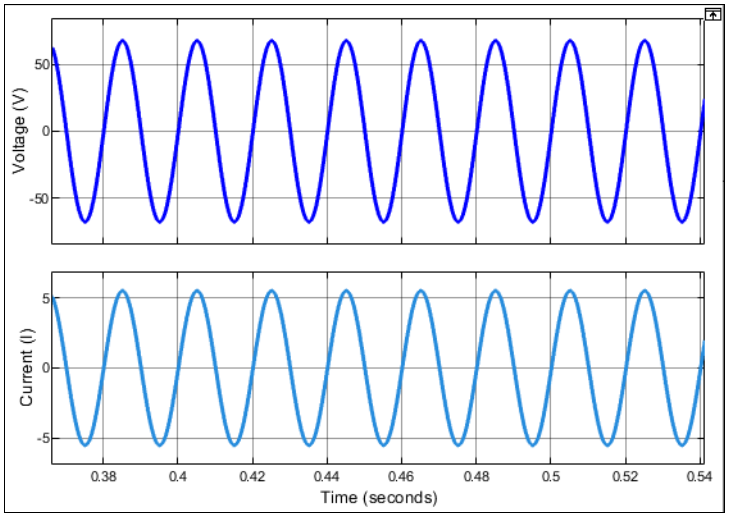

Fig 12: Secondary Side Voltages, Currents

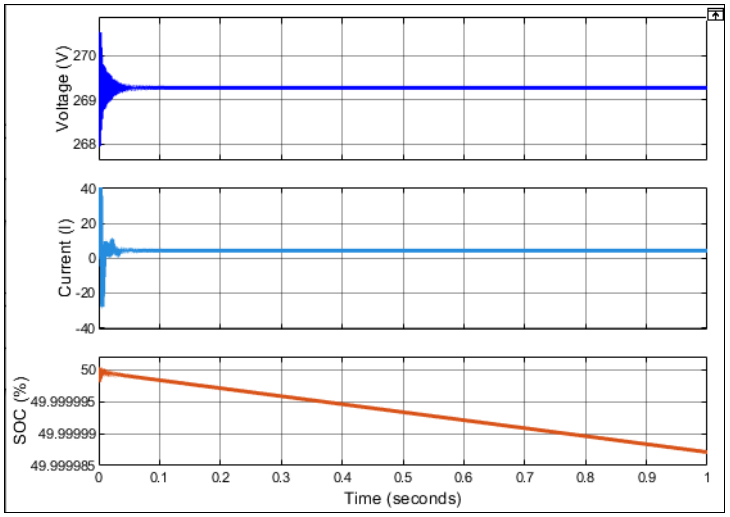

Fig 13: Battery Voltage, Current & SOC

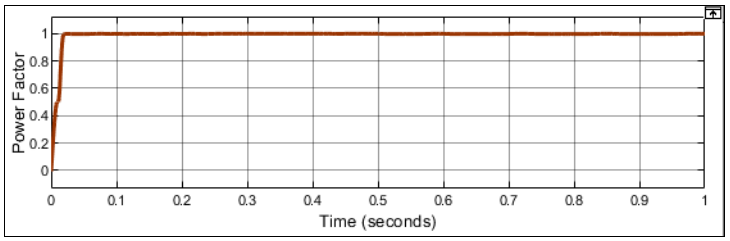

Fig 14: Power Factor

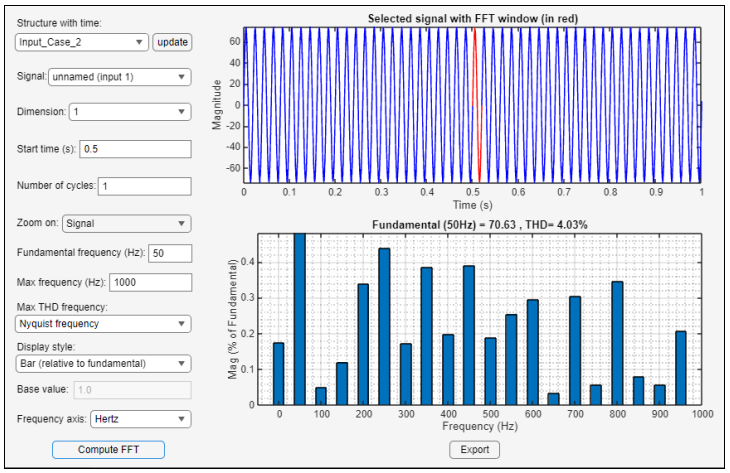

Fig 15: THD's in Grid Voltage

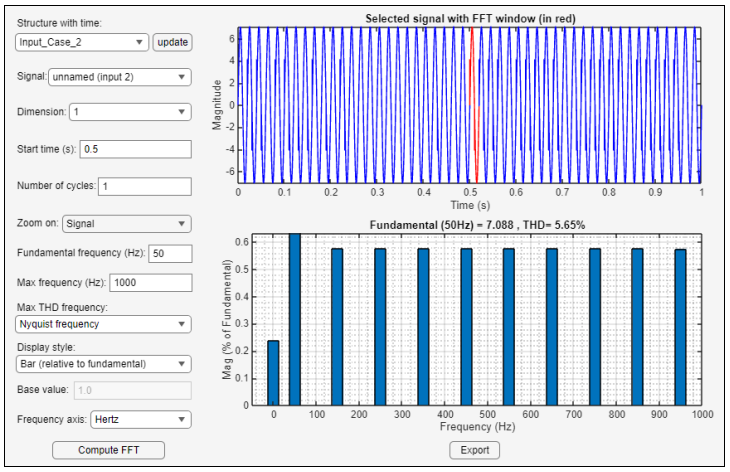

Fig 16: THD's in Grid Current

In the Vehicle-to-Grid (V2G) mode, the situation reverses. When there are power outages or grid power shortages, the EV's battery can supply energy back to the grid. This is done through a DC-AC inverter, which converts the stored DC power in the battery to AC (alternating current) that can be fed into the grid. This feature allows the EV to act as a temporary energy source for the grid, providing power during times of high demand or when the grid is unstable.

Comparison Table

Condition	THD's in Grid Voltage	THD's in Grid Current
G2V	3.82%	4.00%
V2G	4.03%	5.65%

An important aspect of these operations is the Total Harmonic Distortion (THD) levels at the grid side. THD refers to the amount of distortion in the waveform of the current or voltage, which can be caused by non-linear loads like inverters. The diagram demonstrates the variation in THD levels during both G2V and V2G operations.

Results and Discussion

To validate the proposed loss model for the single-stage, single-phase isolated PFC converter used in bidirectional plug-in EV chargers, both simulation and experimental analyses were conducted. The converter prototype, rated at 3.3 kW, operated at a switching frequency of 50 kHz, with a 230 V RMS grid input and a 400 V DC-link output. The loss model accounted for conduction losses in the power switches and diodes, switching losses, transformer core and copper losses, as well as auxiliary losses such as those from gate drivers and control circuitry.

A comparison between the predicted efficiency from the loss model and experimental results shows strong agreement across a range of load conditions. The maximum deviation observed was within ±1.5%, indicating a high level of accuracy. At full load, the predicted efficiency was 95.3%, while the experimentally measured value was 95.1%. This close correlation confirms the effectiveness of the model in estimating the actual performance of the converter.

The analysis of loss distribution under full-load conditions revealed that conduction losses in both the MOSFETs and diodes formed the largest share of total losses. Transformer-related losses, including both core and copper losses, were also significant. Switching losses, though lower in proportion, became more influential at lighter loads and higher frequencies. Auxiliary losses remained relatively minor but non-negligible, particularly in control-intensive applications.

During bidirectional operation, the model maintained its accuracy when applied to discharging mode, where energy flows from the DC link back to the grid. The efficiency in this reverse mode remained nearly identical to that in charging mode, with variations of less than 0.3%. This result highlights the converter's suitability for vehicle-to-grid applications, where symmetric performance in both directions is essential for maximizing energy throughput and minimizing loss.

When compared with conventional loss estimation techniques, which often overlook magnetic losses or assume linear switch characteristics, the proposed model consistently outperformed in accuracy, especially under dynamic and light-load conditions. The comprehensive approach taken by the model allows for more precise system-level optimization and better prediction of thermal performance and reliability over time.

In summary, the proposed loss model has demonstrated a strong correlation with experimental data, validated its applicability across bidirectional modes, and provided valuable insight into where efficiency improvements can be targeted in future designs.

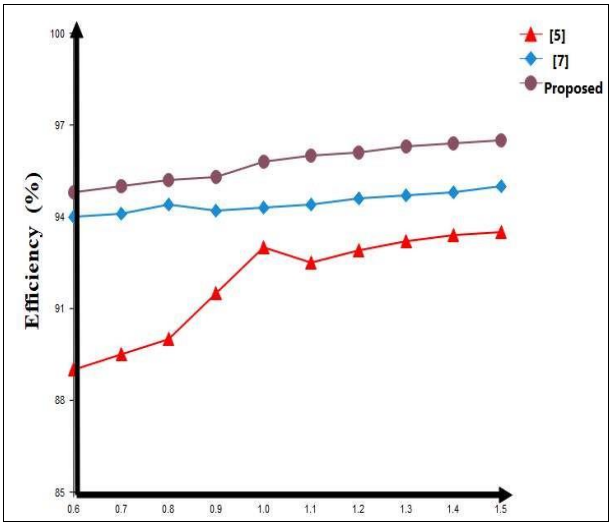

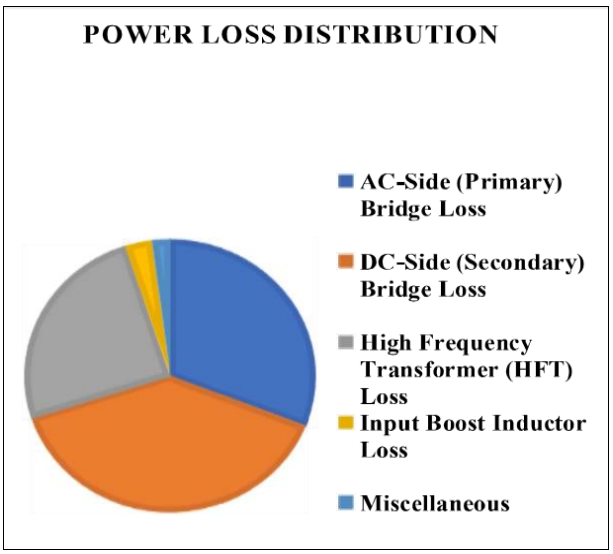

References

1. Williamson SS, Rathore AK, Musavi F. Industrial electronics for electric transportation: Current state-of-the-art and future challenges. IEEE Trans Ind Electron. 2015;62(5):3021-3032. DOI:10.1109/TIE.2015.2409052.
2. Kisacikoglu MC, Ozpineci B, Tolbert LM. EV/PHEV bidirectional charger assessment for V2G reactive power operation. IEEE Trans Power Electron. 2013;28(12):5717-5727. doi:10.1109/TPEL.2013.2251007.
3. Samanta S, Rathore AK. A new inductive power transfer topology using direct AC-AC converter with active source current wavenshaping. IEEE Trans Power Electron. 2018;33(7):5565-5577. DOI:10.1109/TPEL.2017.2750081.
4. Weise ND, Castelino G, Basu K, Mohan N. A single-stage dual active-bridge-based soft switched AC-DC converter with open-loop power factor correction and

other advanced features. IEEE Trans Power Electron. 2014;29(8):4007-16. doi:10.1109/TPEL.2013.2293112.
5. Li C, Zhang Y, Cao Z, Xu D. Single-phase single-stage isolated ZCS current-fed full-bridge converter for high-power AC/DC applications. IEEE Trans Power Electron. 2017;32(9):6800-6812. DOI:10.1109/TPEL.2016.2623771.
6. Salmon JC. Circuit topologies for single-phase voltage-doubler boost rectifiers. In: Proc IEEE Appl Power Electron Conf Expo; 1992. p. 549-556.
7. Musavi F, Eberle W, Dunford WG. A phase-shifted gating technique with simplified current sensing for the semi-bridgeless AC-DC converter. IEEE Trans Veh Technol. 2013;62(4):1568-1576.
8. Kim Y, Sung W, Lee B. Comparative performance analysis of high density and efficiency PFC topologies. IEEE Trans Power Electron. 2014;29(6):2666-2679.
9. Liu Z, Lee FC, Li Q, Yang Y. Design of GaN-based MHz totem-pole PFC rectifier. IEEE J Emerg Sel Top Power Electron. 2016;4(3):799-807.
10. Liu Z, Huang Z, Lee FC, Li Q. Digital-based interleaving control for GaN-based MHz CRM totem-pole PFC. IEEE J Emerg Sel Top Power Electron. 2016;4(3):808-814.
11. Lee IO, Moon GW. Half-bridge integrated ZVS full-bridge converter with reduced conduction loss for electric vehicle battery chargers. IEEE Trans Ind Electron. 2014;61(8):3978-3988. DOI:10.1109/TIE.2013.2282608.
12. Prasanna UR, Singh AK, Rajashekara K. Novel bidirectional single-phase single-stage isolated AC-DC converter with PFC for charging of electric vehicles. IEEE Trans Transp Electrif. 2017;3(3):536-544. DOI:10.1109/TTE.2017.2691327.
13. Rathore AK, Prasanna UR. Analysis, design, and experimental results of novel snubberless bidirectional naturally clamped ZCS/ZVS current-fed half-bridge DC/DC converter for fuel cell vehicles. IEEE Trans Ind Electron. 2013;60(10):4482-4891. DOI:10.1109/TIE.2012.2213563.
14. Pan X, Li H, Liu Y, Zhao T, Ju C, Rathore AK. An overview and comprehensive comparative evaluation of current-fed-isolated bidirectional DC/DC converter. IEEE Trans Power Electron. 2020;35(3):2737-2763. DOI:10.1109/TPEL.2019.2931739.
15. Pan X, Rathore AK. Novel bidirectional snubberless naturally commutated soft-switching current-fed full-bridge isolated DC/DC converter for fuel cell vehicles. IEEE Trans Ind Electron. 2014;61(5):2307-2315. DOI:10.1109/TIE.2013.2271599.
16. CREE. C2M0040120D SiC MOSFET Technology. 2022 [cited 2025 Apr 18]. Available from: https://assets.wolfspeed.com/uploads/2020/12/C2M0040120D.pdf
17. Magnetics. Powder core loss calculation guide. 2022 [cited 2025 Apr 18]. Available from: https://www.mag-inc.com/design/designguides/powder-core-loss-calculation
18. TDK. High frequency transformer (HFT) design. [cited 2025 Apr 18]. Available from: https://product.tdk.com/system/files/dam/doc/product/ferrite
19. Patel N, Lopes L, Rathore AK. Analysis and design of soft switching single-stage single-phase PFC converter for bidirectional plug-in EV charger. In: Proc IEEE Energy Convers Congr Expo (ECCE); 2022.